Kinetik: Game Technology, Information System, Computer Network, Computing, Electronics, and Control
Journal homepage: http://kinetik.umm.ac.id
ISSN: 2503-2267
Vol. 10, No. 2, May, Pp. 115-134

PID controller-based simulations for controlling inverter voltage to enhance power in a microgrid

Reza Maulidin*[1], Bayu Rahmad Nugroho[1], Adhi Kusmantoro[1]
Department of Electrical Engineering, Universitas PGRI Semarang, Indonesia[1]

Article Info

Keywords:
Voltage control, Solar Inverter, PID, PV ARAY

Article history:
Received: August 29, 2024
Accepted: January 03, 2025
Published: May 31, 2025

Cite:
R. Maulidin, B. R. Nugroho, and A. Kusmantoro, "PID Controller-Based Simulations for Controlling Inverter Voltage to Enhance Power in a Microgrid", *KINETIK*, vol. 10, no. 2, May 2025. https://doi.org/10.22219/kinetik.v10i2.2106

*Corresponding author.
Reza Maulidin
E-mail address:
rezamaulidin@upgris.ac.id

Abstract

An inverter is a device that converts direct current (DC) into alternating current (AC), which is crucial in various applications, including solar power systems, uninterruptible power supplies (UPS), and electric motor control. Accurate and stable voltage control of the inverter is essential to ensure the performance and reliability of the system. The Proportional-Integral-Derivative (PID) control method is one of the most commonly used control techniques due to its simplicity and effectiveness across different control systems. This study focuses on the implementation of inverter voltage control using a PID controller. The PID controller is designed to regulate the inverter's output voltage, ensuring stability even in the presence of disturbances or load variations. In this research, the mathematical model of the inverter and the PID control system is developed and simulated using MATLAB/Simulink software. The simulation results demonstrate that the PID controller effectively maintains the inverter's output voltage, providing a rapid transient response with minimal overshoot. The application of the PID controller to the inverter also shows improvements in system stability and a reduction in steady-state error. Furthermore, precise tuning of the PID parameters is a key factor in achieving optimal control performance. This research makes a significant contribution to the field of inverter control by demonstrating the effectiveness of the PID controller in regulating the inverter's output voltage. The practical implementation of PID controllers on inverters is expected to enhance the efficiency and reliability of power systems that utilize inverters.

1. Introduction

In the era of rapid technological advancements and increasing demand for stable electricity sources, effective inverter control techniques have become a critical aspect of microgrid systems. This necessity is further emphasized by the depletion of fossil fuel resources, which has accelerated the transition to renewable energy. Microgrids, as distributed generation systems leveraging renewable energy, provide a viable solution to meet society's growing need for stable electrical power. This research focuses on distributed generation and the development of converters. Voltage control of inverter plays a pivotal role in electrical power systems. In each control cycle, twenty-seven voltage vectors are evaluated using a predictive model to determine the optimal and suboptimal switching states, with the optimal state selected within two control cycles. To address sampling and computation delays, the FCS-MMPVC algorithm incorporates delay compensation. Simulation and experimental results demonstrate that this method ensures good stability and reliability. Compared to the conventional FCS-MPC algorithm, this approach significantly reduces the deviation between output voltage and reference under unbalanced and non-linear load conditions, thereby enhancing the quality of the inverter's output voltage[1].

In distributed generation systems, variations and the effects of nonlinear loads can significantly degrade the control performance. Improper load disturbances negatively impact the inverter system through different control input channels. To address this, a harmonic disturbance observer (HDOB) is proposed to estimate periodic load disturbances. With this new compensation for these disturbances, the negative impact on the output voltage can be eliminated [2]. Overvoltage is one of the challenges in distribution networks with high photovoltaic (PV) penetration. Centralized or distributed Active Power Curtailment (APC) methods and/or PV reactive power control are viable solutions to prevent overvoltage. This article proposes two distributed methods to control PV inverters based on nodal sensitivity. The performance of the proposed methods is then compared with two commonly used control methods [3]. To achieve optimal control, an enhanced Linear Active Disturbance Rejection Controller (LADRC) is employed to regulate the outer-loop voltage. First, the mathematical model of the inverter connected to the wind power grid is analyzed. Based on this analysis, the linear active disturbance rejection control is designed using a reduced-order linear state observer, which reduces phase lag and improves the accuracy of system disturbance observation. A lead-lag correction method is applied to enhance observer gain and reduce the effects of noise amplification. Frequency domain response analysis demonstrates that the enhanced LADRC possesses superior disturbance rejection capabilities [4]. An adaptive DC-link voltage control method is proposed for two-stage photovoltaic (PV) inverters during low voltage ride-through (LVRT) operation. The DC-link voltage will be adjusted in response to grid voltage changes during LVRT to maintain a high modulation ratio, thereby reducing the high-frequency harmonics injected into the grid. Additionally, under asymmetric grid faults, this control method can reduce the double-frequency ripple in the DC-link voltage and keep the DC-link voltage within a safe range by shifting the double-frequency power ripple to the front end of the DC input source. This can be achieved by regulating the DC input power fluctuations or using a bidirectional DC-DC converter depending on the voltage drop ratio and input power level [5], [6]. In a microgrid, Voltage Source Inverters (VSI) in Distributed Generation (DG) units can operate in either Voltage Control Mode or Current Control Mode (VCM/CCM). VCM and CCM are utilized for reactive power sharing and voltage harmonic compensation. This decentralized control scheme relies on local signal measurements, eliminating the need for communication links and simplifying the system structure. The VCM units use virtual capacitive impedance for harmonic compensation, addressing the effects of the LCL filter output inductance. CCM units regulate adaptive virtual input based on the remaining capacity. Modified droop and reverse droop control methods are applied for reactive power sharing [7], [8]. Fault management strategies are crucial for the operation of distribution networks. This includes current and voltage limiting strategies to enhance the fault ride-through (FRT) capability in inverter-based microgrids (MGs) operating in islanded mode, considering the effects of inverter control systems and inverter topology (four-wire/three-wire configurations). A three-phase voltage source inverter with a multi-loop control system is employed in both synchronous and stationary references for four-wire and three-wire configurations. This strategy ensures high voltage and current quality during overcurrent conditions, which is essential for sensitive loads [9]. Consensus-based distribution voltage control (DVC) addresses the issue of reactive power sharing in autonomous inverter-based microgrids with inductive power lines and arbitrary topologies. Unlike other control strategies, DVC ensures stable reactive power distribution by requiring only distributed communication among inverters, without the need for centralized computation or unit communication. For inductive impedance loads and assuming small phase angle differences between inverter voltage outputs, the choice of control parameters determines the closed-loop voltage equilibrium point and reactive power dynamics. Necessary and sufficient conditions for local exponential stability are also provided for measurement filters with uniform power time constants [10]. Potential balancing control is achieved by sampling the voltage of separate dc-link capacitors and then adjusting the modulation waveform based on the voltage differences. This paper proposes an NP open-loop potential balancing control for full-bridge grid-connected inverters (FB-GCIs) with 5L-NPC. A balancing factor, k is incorporated into the modulation signal and adjusted according to the modulation index. Thus, even though the dc-link capacitor voltage is not directly sampled and controlled, the capacitor voltages remain balanced across a wide modulation index range [11], [12]. The LCL filter is used as an interface between the inverter and the power grid, but it requires a damping method to address filter resonance. Inverter-side current feedback (ICF) control incorporates over-current protection and active damping. Some literature suggests that capacitor voltage feed-forward (CVF) can enhance the stability of ICF control. However, implementing ICF with CVF encounters two issues: CVF tends to cause low-frequency oscillations, especially in weak grids, and low-frequency harmonics in the grid voltage can distort the inverter's grid-side current. To address these issues, a new inverter-side current control method is proposed, which involves adding a high-pass filter to the CVF path [13], [14], [15], [16], [17]. A disturbance observer-based fuzzy sliding mode control (DOBFSMC) strategy is proposed for a single-phase inverter connected to a PV grid. Uncertainties arising from variations in inverter component parameters and changes in climatic conditions can impact control performance. The disturbance observer estimates disturbances in real time, and the sliding mode controller uses this information to regulate the DC-AC inverter output voltage. The fuzzy system estimates the upper bound of the error between the actual disturbance and its observed value to enhance inverter performance. As a result, the inverter becomes more resilient to disturbances, and switching gain can be minimized due to the fuzzy system's estimation of the error bound [18]. An adaptive fuzzy neural network control (AFNNC) is proposed for a single-stage boost inverter. The dynamic model of the inverter is analyzed for control manipulation. A total sliding mode control (TSMC) framework without the reaching phase is developed to enhance system robustness during transient responses. To mitigate control chatter due to the sign function in TSMC, the AFNNC system is used to approximate the TSMC law. The online learning algorithm in AFNNC is based on Lyapunov stability theory and projection algorithms, ensuring stability without the need for additional compensation controllers despite uncertainties. The AFNNC output can be directly supplied to the power switch cycle in the boost inverter without stringent constraints on control parameters [19]. The decentralized control architecture for inverters in an interactive utility autonomous microgrid consists of multiple inverter units. Its key features include automatic transitions between grid-connected and islanded operation modes, islanding/anti-islanding detection, low voltage ride-through (LVRT), and grid support with reactive power injection (RPI). Three primary control loops—voltage, frequency, and phase-locked loop (PLL)—are designed within a synchronous reference frame (SRF) for simplicity and efficiency. The equivalent droop integrates virtual resistance with active (P) and reactive (Q) power-based droops for proportional load sharing in islanded mode. Each inverter operates with its terminal information, eliminating the need for centralized controllers or communication networks [20]. Adaptive DPWM control for a three-level inverter with two PV panel strings in a cascaded connection is proposed. This modulation is based on the concept of circuit-level decoupling, which ensures that the line voltages remain balanced even if the DC link is unbalanced. The DC voltage imbalance is addressed by asymmetrical MPPT controlled through zero-sequence voltage injection into the common-mode voltage, while the total DC voltage is regulated according to the voltage commands from each MPPT. This approach allows both PV strings to operate based on their respective MPPTs with minimal low-frequency harmonic distortion in the inverter output current [21]. Solar power plants are considered a better alternative energy source, but they come with problems and weaknesses. Issues encountered include insufficient power generation with low efficiency, high oscillations, and very slow power tracking. To address these issues, a combination of P&O-fuzzy and IC-fuzzy methods is used in the design. Additionally, the combined algorithm can deliver better performance compared to conventional algorithms due to its effective duty cycle performance according to the system design [22]. One of the major limitations of the classical Interconnection and Damping Assignment Passivity-Based Control (IDA-PBC) approach is its reliance on system parameters. To address this, the proposed method improves load voltage quality under both nominal conditions and scenarios involving system uncertainties. The power system is modeled within the framework of a Port-Controlled Hamiltonian (PCH) system, and the control design process is thoroughly detailed [23]. Coordinating superconducting fault current limiters (SFCL), superconducting magnetic energy storage (SMES), and distributed generation (DG) units enhances microgrid stability during short-circuit faults. This control enables smooth disconnection from the main grid during severe faults and fault ride through (FRT) during minor faults. A fuzzy logic controller is used for the SFCL, replacing the PI controller to reduce fluctuations more effectively [24]. The approach involves designing multi-inverter controllers for both the solar power source and the battery system. The proposed microgrid is integrated with the utility grid, comprising multiple inverters connected to individual battery units and solar panel outputs. Single-phase inverters, tailored for residential applications, are employed. To regulate the output of each inverter, a coordination control strategy based on Fuzzy Logic Controller (FLC) is implemented [25], [26], [27], [28], [29]. The system is designed to mitigate harmonics and manage reactive power within the power network. A self-tuning perturb and observe (SPO) algorithm is employed to optimize maximum power tracking in the PV array. The SHAF incorporates a maximum M Kalman filter (MMKF) to estimate reference currents, while hysteresis current control (HCC) is used to generate switching signals [30]. A centralized DC microgrid approach is proposed to meet household electricity demands, utilizing renewable energy sources. This method employs a centralized system coupled with battery storage, where excess energy generated by rooftop PV systems is stored. In the event of a disconnection of a household's PV system, the battery supplies the necessary power. The findings indicate that the centralized load system requires only total load data, while in a distributed load system, batteries are utilized to meet peak load demands for individual loads [31]. This paper proposes a coordinated and predictive voltage control method for power distribution systems with high penetration of photovoltaic (PV) units. Initially, integrated voltage regulation is achieved through coordination of the voltage regulator (VR) tap position and distributed reactive power control of the PV inverter outputs, ensuring the system voltage remains within acceptable limits. Additionally, solar power forecasting is utilized to anticipate voltage fluctuations, enabling proactive adjustments to the VR tap settings and capacitor switch status, thereby minimizing large voltage deviations [32]. Optimal control can mitigate voltage, current, and power flow issues between the Grid and Distributed Generation (DG) units. By balancing power distribution among parallel-connected DGs, the system compensates for unwanted voltage and current components. Power Quality Conditioners and DG inverters serve dual roles: injecting power from DGs into the Grid and acting as Parallel Active Power Filters to address harmonics, imbalances, and active/reactive power needs for both balanced and unbalanced loads. These functions can be performed individually or in grid-connected mode [33]. The microgrid storage system provides essential on-demand services, utilizing high-energy-density lithium-ion batteries. It consists of three PV array units, each with two PV arrays and two batteries. These batteries store energy from the PV arrays and the single-phase AC grid. The PV arrays output 22.8 V, while the batteries provide 22.78 V. A boost converter raises the voltage to 48 V DC, and a PID controller effectively manages voltage regulation [34]. In this study, a fuzzy PID approach will be implemented as the MPPT controller for the PV system. Fuzzy logic is employed to enhance the PID performance in tracking the maximum power point, ensuring stable voltage or output power from the boost converter. The fuzzy inputs are power and irradiation, while the output is the adjustment of PID parameters to regulate the boost converter effectively [35]. An innovative approach is proposed in this paper. The Residential Power Router (RPR) consists of a dual-half bridge (DHB) converter and a split-phase inverter. The DHB provides galvanic isolation and a bidirectional power flow channel for the distributed generation terminal. The split-phase inverter functions as an active power filter, a reactive power compensator, and balances power between two phases. The power balancing mode is crucial for residential microgrids, especially when the utility grid is unavailable [36]. The proposed control method offers adaptable power-sharing strategies to manage fluctuations in renewable energy sources (RES) and ensure frequency and voltage regulation for each distributed generation (DG) unit. Eigenvalue analysis and time-domain simulations indicate that at high wind speeds and solar irradiance, the damping ratio of critical modes and the dynamic performance of DG units vary significantly [37]. A method is proposed to mitigate voltage imbalance when Distributed Generation (DG) is disconnected from the grid. Control loops associated with voltage and frequency power are implemented to regulate local load voltage and frequency. Additionally, a virtual impedance loop and a proportional-resonant controller are employed within the control framework [38]. A multi-master-slave control strategy is proposed for the interface converters of Distributed Generators (DG) within a three-phase, four-wire islanded microgrid, utilizing Conservative Power Theory (CPT). Inverters located in close proximity operate as a group in a master-slave configuration[39]. DG inverters can be utilized to address power quality issues such as harmonics, reactive power compensation, and imbalances in power distribution systems. These inverters are referred to as multifunctional grid-tied inverters (MFGTI) [40].

Previous research on inverter voltage control has highlighted challenges in achieving adequate stability and reliability, especially under unbalanced and nonlinear load conditions. These shortcomings often lead to degraded system performance, including prolonged settling times, high overshoot, and reduced precision in voltage regulation. To overcome these issues, this study introduces a PID (Proportional-Integral-Deriative) controller as an innovative solution. A PID controller offers numerous advantages, including faster response time, higher accuracy in handling load variations and system disturbance, and more adaptive to various operational conditions. These advantages make PID controller a more reliable and efficient choice compared to other conventional method like PI controller or other advanced technique. By leveraging these methods, the proposed system ensures voltage stability, mitigates power quality issues, and maintains optimal operational performance under dynamic conditions. Based on the introduction, the structure of this article is compiled as follows: Section 2 outlines the Research Methodology, Section 3 presents the Results and Analysis, and Section 4 concludes with the Final Remarks.

2. Research Method

2.1 PV ARAY

The power performance of a PV array is influenced by solar irradiance and ambient temperature. The output power in this model is expressed by Equation 1.

$$P_{pv} = \eta_{pv} \times A_{PV} \times I_r \tag{1}$$

According to Equation 1, the output power of the PV(P_{pv}) depends on the PV production efficiency (η_{pv}), the cross-sectional area of the PV (A_{pv}), and the solar irradiance (I_r). The PV production efficiency (η_{pv}) is influenced by the module efficiency (η_r) and the power conditioning efficiency (η_{pc}). The module efficiency (η_r) is dependent on the temperature coefficient (β) and the difference between the cell temperature (T_c) and the reference cell temperature (T_{cr}), as described in Equation 2.

$$T_{cr} = T_a \times \eta_{pc} \left[1 - \beta(T_c - T_{cr}) \right] \tag{2}$$

The temperature coefficient (β) ranges from 0.004 to 0.006 per °C. The cell's reference temperature (T_{cr}) is significantly influenced by changes in ambient temperature (T_a). Additionally, the impact of solar radiation intensity (I_r) in this equation is also dependent on the cell's nominal operating temperature (T_{op}) [29]. Photovoltaic (PV) panels primarily consist of numerous modules interconnected in series and parallel configurations to achieve the desired voltage and current levels. To accurately model and design these modules mathematically, the single-diode model is typically employed. In electrical terms, this model is represented by an equivalent circuit comprising a current source, a parallel diode, series resistance (Rs), shunt resistance (Rsh), and bypass diodes arranged in an anti-parallel configuration. The current-voltage (I-V) characteristics of the PV module can be expressed by the Equation 3.

$$I = I_{ph} - I_O \times (\exp\left(\frac{V+IR_s}{{}_nV_T}\right) - 1) - \frac{V+IR_s}{R_{sh}} \tag{3}$$

In this equation, I represents the output current of the module, V is the output voltage, I_{ph} is the generated photocurrent, I_O is the diode's reverse saturation current, n is the ideality factor, V_T is the thermal voltage, R_s is the series resistance, and R_{sh} is the shunt resistance. The parameters I_M, V_M, I_{ph}, I_O, F and V_T correspond to the module's maximum current, maximum voltage, generated photocurrent, diode current, ideality factor, and thermal voltage, respectively. The series-parallel (SP) configuration is the most commonly used and widely adopted setup for PV arrays. In this arrangement, individual modules are first connected in series to increase the voltage, forming what are known as strings. These strings are then connected in parallel to amplify the current. This configuration is favored for its simplicity and ability to scale both voltage and current to meet the desired power output.

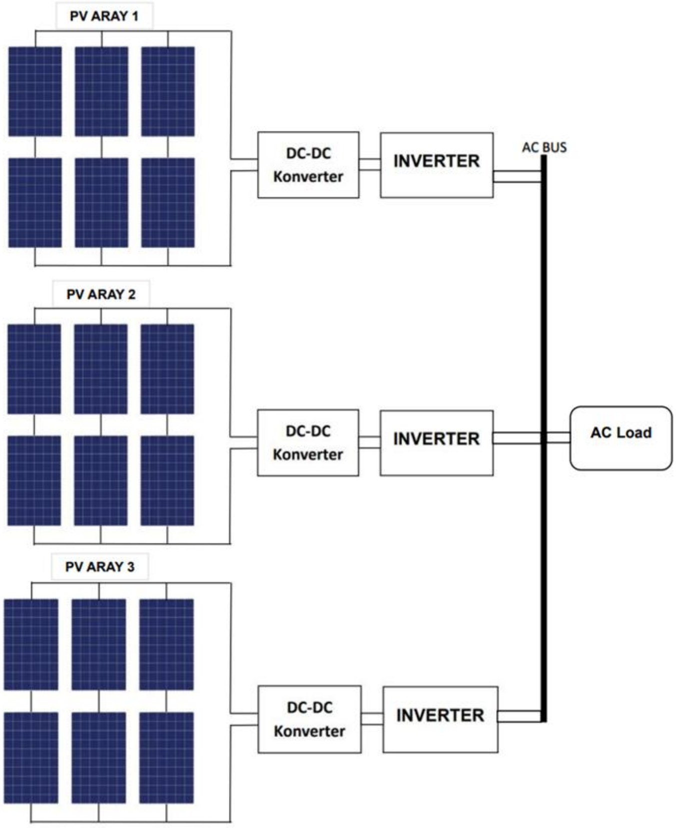

Figure 1. PV Aray System

The specifications of the PV module depicted in Figure 1 under Standard Test Conditions (STC)—defined by an irradiance of 1000 W/m² and an operating temperature of 25°C—are presented in Table 1. To ensure the validity of the experimental results, simulations were conducted by considering real-time environmental conditions, wherein the PV module experienced a peak irradiance of 800 W/m² and a module temperature of 45°C under normal operating conditions.

Table 1. Ratings of the PV Module at Different Conditions, i.e., STC and NOCT

Parameters	Rarings	
	At STC	*At Fiedd Condition*
Rated Peak Power (Pmax)	100 W	84.55
Voltage at Maximum Power (VMP)	18.6 V	16.09
Current at Maximum Power (IMP)	5.37 A	5 A
Open-Circuit Voltake (VOC)	22.8 V	20.35 V
Shot-Circuit Current (ISC)	5.71 A	3.50 A
Fill Factor (F.F)	74.69 %	72.16 %
Efficiency	16.83 %	14.54 %
Fuse Rating	15 A	
Maximum System Voltage	600 V	
Dimension	600 X 800 mm	
Power Tolerance	±5%	

The effectiveness of array configurations is analyzed through several measurement parameters, focusing on their performance under shaded conditions. One of the primary metrics for this analysis is the power output of the array (PA), calculated using the formula in Equation 4.

$$PA = VA \times IA \tag{4}$$

The mismatch loss (ML) encountered during shading is determined by the difference between the power output of an unshaded array (PU) and a shaded array (PS), as described by Equation 5.

$$ML = PU - PS \tag{5}$$

The power loss percentage (PL) under shading is derived from Equation 6, with PSTC representing the power output under Standard Test Conditions (STC).

$$PL(\%) = \frac{PSTC - PS}{PSTC} \times 100 \tag{6}$$

The array configuration efficiency (ηPG) is calculated using Equation 7, where ‘G’ represents irradiance, and ‘A’ represents the module's receiving area.

$$\eta PG(\%) = \frac{PS}{PC} \times 100 \tag{7}$$

Finally, Equation 8 expresses the performance ratio (PR) for array configurations under shading conditions as the percentage ratio of the shaded power output to the unshaded power output.

$$PR(\%) = \frac{PS}{PU} \times 100 \tag{8}$$

2.2 Grid Inverter

The classification of grid inverter systems can be divided into four types according to the control methods: voltage sources regulated by voltage, voltage sources regulated by current, current sources regulated by voltage, and current sources regulated by current. In current source inverters, a substantial inductance is necessary on the DC side to maintain input stability. However, this can significantly hinder the system's dynamic response. Consequently, voltage source inputs have become the preferred choice for most modern grid inverters.

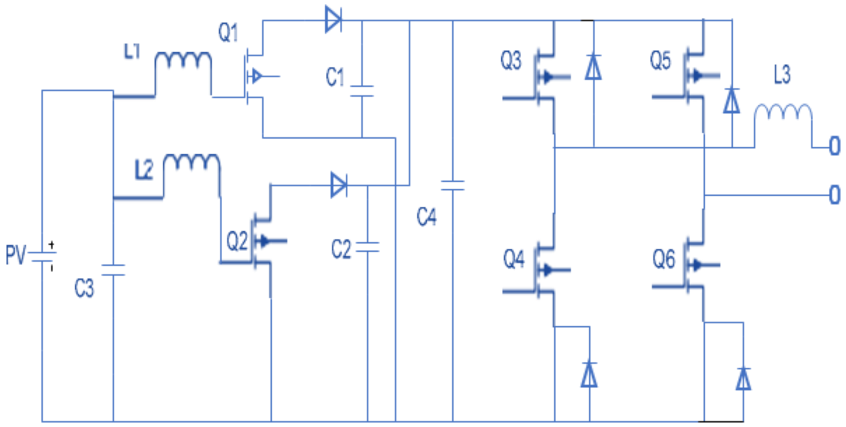

Figure 2. The Main Circuit Structure

The topology diagram of the system's hardware structure, as shown in Figure 2, includes several key components: Q3 to Q6 are IGBT switches, D3 to D6 serve as free-wheeling diodes, L1 and L2 are filter inductors, UAB(t) represents the output voltage of the inverter, Unet(t) is the sinusoidal voltage from the power grid, and iL(t) is the grid current generated by the inverter. The grid voltage can be expressed by Equation 9.

$$\mathrm{Unet} = \mathrm{UAB} - \mathrm{j} * \dot{\mathrm{A}}\mathrm{N} * \mathrm{LN} * \mathrm{IL} \tag{9}$$

ȦN represents the angular frequency, with ȦN = 2π * fN, and fN are frequency. The Equation 10 represents the relationship between the current $I(s)$ and the input voltage $U_{net}(s)$ in the Laplace domain. Here, G(s) is the system's transfer function, which describes the dynamic behavior of the system. The term $\frac{1}{1+G(s)}$ acts as a scaling factor that determines how the input voltage is translated into the system's current. This formulation is commonly used in control systems to model feedback and system stability.

$$\mathrm{I(s)} = \frac{1}{1+G(s)} \cdot U_{net(s)} \tag{10}$$

When grid voltage feed-forward control is applied, the effect of the voltage on the grid current can be described by Equation 11 as follows.

$$\mathrm{I(s)}=\frac{1}{1+G(s)} \cdot \frac{1+G_n(8)G(8)}{1+G_2(8)} . U_{net}(s) \tag{11}$$

Based on Equations 1-3, the transfer function can be determined as follows. This transfer function is crucial for understanding the system's response and stability, allowing for precise control and optimization of the inverter's performance.

$$G_{spwm}(s) = \frac{1}{k_1 8 + k_2} \tag{12}$$

$$G_n(s) = \frac{G_1(s)}{G_2(s) - 1} \tag{13}$$

When $I(s = 0)$, the voltage control of the inverter can be effectively implemented, as illustrated in the figure. This implementation ensures that the inverter maintains optimal performance under the specified conditions, as described by Equations 12 and 13. Equation 12 represents the transfer function $G_{spwm}(s)$, while Equation 13 depicts the relationship between $G_n(s), G_1(1)$,and $G_2(s)$.

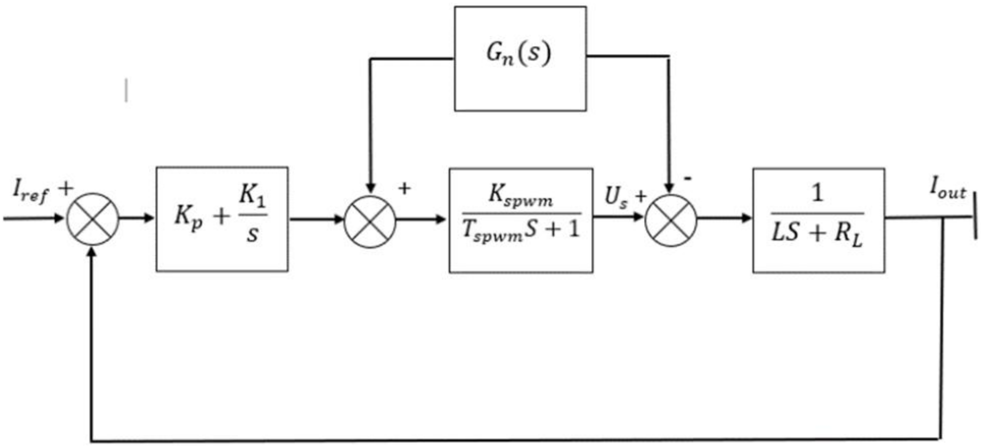

Figure 3. The Voltage Feed Forward Closed-loop Control structure

Figure 3 illustrates the closed-loop control structure with voltage feed-forward. It can be concluded that the voltage feed-forward control method effectively mitigates the impact of voltage variations on the output current, theoretically achieving full compensation. This approach ensures enhanced accuracy and stability in the inverter's performance.

2.3 Voltage Regulation for PV Inverters Using PID Control

Contemporary inverters are increasingly capable of providing reactive power to the grid and regulating feeder voltage in addition to generating active power from their photovoltaic (PV) cells. This capability, where the inverter's performance is depicted as a vector with magnitude of SSS; the semicircle with SSS radius defines the operational limits of the inverter within the PQ space. Assuming that the PV array generates power at PPVP_{PV}PPV, the reactive power (Q) limits are determined by projecting the endpoints of the power vector onto the Q axis. Compared to fixed capacitors, inverters offer the advantage of continuously adjustable reactive power, with a regulation response that is notably faster—typically within 3-5 cycles—compared to conventional voltage regulation devices.

Given their capability to supply reactive power, PV inverters can implement automatic voltage regulation techniques. These techniques operate within a designated voltage range using a PID controller. When the voltage at the measurement point deviates from this range, the PV inverter will either inject or absorb reactive power to bring the local voltage back to its normal range. Consistent with the principle of prioritizing active power, the PID controller ensures that voltage regulation is both efficient and responsive to fluctuations in voltage conditions, maintaining system stability while adapting to operational demands.

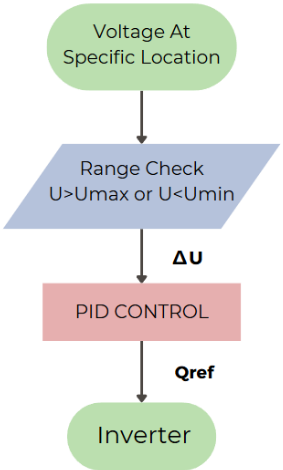

Figure 4. Diagram Illustrating the Techniques for Automatic Voltage Regulation

Table 2. Common Control Methods

Control	Attributes
$Q(U)$	Reactive power as a function of voltage
$PF(P)$	Power factor as a function of the delivered active power
$P\&\,Q(U)$	Integration of $P(U)$ and $Q(U)$ functions
$PF(P)\&P(U)$	Integration of $PF(P)$ and $P(U)$ functions
$P(U)$	Active power reduction based on voltage levels
Optimal Power Flow	Optimize the net photovoltaic power while adhering to power flow constraints

The reactive power supplied by the inverter must be constrained within the range of $(Q_{limit}\ to\ Q_{limit})$, as defined by Equation 14.

$$Q_{limit} = \sqrt{S^2} - P_{PV}^2 \tag{14}$$

Figure 4 illustrates a block diagram depicting the automatic voltage regulation techniques employed in inverters. The closed-loop control primarily aims to manage the voltage profile within established limits, rather than maintaining it at a specific reference value, as seen in set-point voltage control mode, which requires the inverter to hold the voltage at a fixed level. However, it is often challenging to keep the local voltage within the desired range due to the reactive power limitations of the inverter and the significant interactions among the voltages at adjustment buses. Therefore, common voltage regulation methods for inverters involve making reactive power a function of either local active power production, Q(P), local voltage, Q(U), or a combination of both. Table 2 summarizes these prevalent voltage control methods used in low-voltage (LV) networks.

In this study, to provide a comprehensive understanding of how inverter-based voltage control methods and their parameters affect the enhancement of Hosting Capacity (HC), two fundamental voltage regulation techniques have been selected and analyzed, as opposed to all the methods listed previously. These techniques are Q(U) – Reactive Power Based on Grid Voltage and PF(P) – Power Factor Based on Active Power. These control strategies lead to distinct reactive power flows within LV feeders. Figure 5 illustrates the reactive power flows associated with load and control for these two strategies.

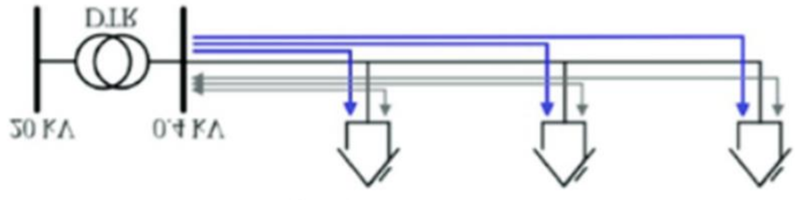

(a)

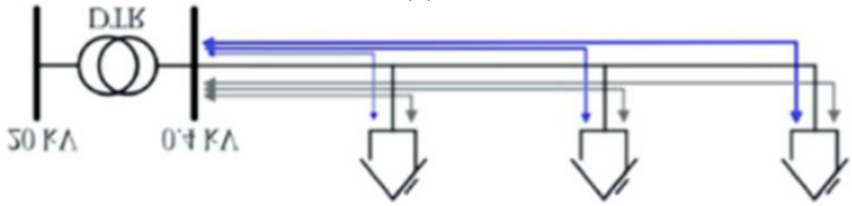

(b)

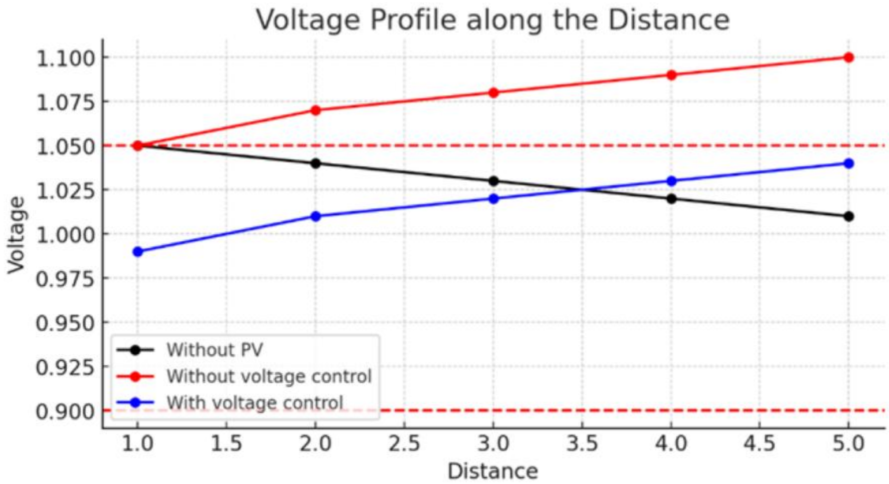

(c)

Figure 5. Load and Control Related Power Flows of Different Control Methods and Relative Voltage Along the Feeder: (a) PF (P) Control; (b) Q(U) Control; (c) Voltage Profile

Figure 5a depicts the scenario under local PF(P) control. In this case, all inverters absorb the same amount of control-related reactive power, assuming identical PV power production conditions (such as irradiance, temperature, tilt angle of PV modules, etc.) along the LV feeder, and uniform PV module and inverter ratings among all consumers. In contrast, under Q(U) control, distributed inverters absorb varying amounts of control-related reactive power based on their local grid voltage, as shown in Figure 5b. Both methods result in uneven control-related reactive power flows through the line segments, leading to different voltage regulation outcomes. Based on Figure 5c, the voltage distribution along the feeder can be observed under three different scenarios: a low-voltage (LV) network without PV, a PV system without voltage control, and a PV system with voltage control.

2.3.1 Reactive Power Control by Grid Voltage

The primary objective of implementing the Q(U) control algorithm is to utilize the inverter's reactive power to regulate voltage effectively. In scenarios where overvoltage occurs, the control system reduces the voltage to a certain level, while in undervoltage conditions, it works to increase the voltage towards a specified target value.
Typically, the Q(U) control is applied as illustrated in Figure 6.

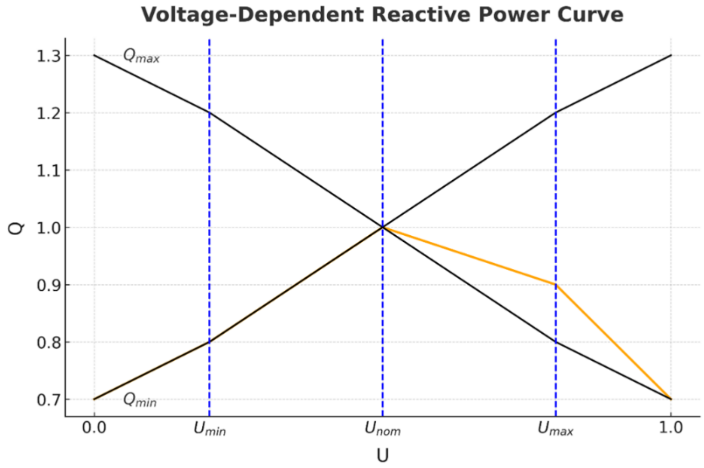

Figure 6. Generic Q(U) Curve and Defining Parameters

The voltage at the inverter's bus terminals serves as an input value for the PID controller. The slope mmm of the Q(U) characteristic curve indicates the sensitivity of the reactive power controller to voltage fluctuations, as described by Equation 3. For instance, if the voltage at the measurement point is slightly above the desired operational range, the PID control adjusts the capacitive reactive power to bring the voltage back within the desired range.

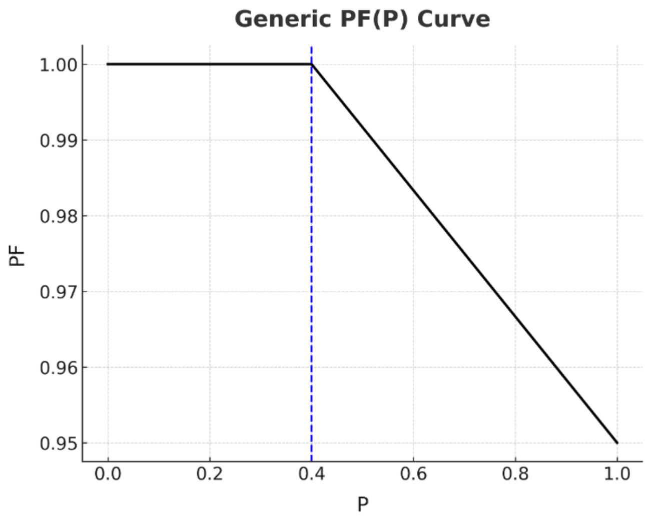

Figure 7. Generic PF (P) Curve

The PID controller is employed to regulate the reactive power supplied by the inverter, ensuring effective voltage management. The maximum limits for the inverter's reactive power can be determined based on its specifications and operational capacity. Figure 7 illustrates a generic PF(P) curve, which serves as a reference for determining the inverter's reactive power contribution as active power increases. The slope *m* in PID control can be expressed by Equation 15.

$$m = \frac{1}{Q}\frac{1}{U} = \frac{Q_{max} - Q_{min}}{U_{max} - U_{min}} \tag{15}$$

The parameters $U_{d,min}$ and $U_{d,max}$ define the voltage deadband within which the PID controller should not produce reactive power. This deadband helps prevent the inverter from injecting unnecessary reactive power. In the PID control method without a deadband, the reactive power $Q(U)$ is calculated as shown in Equation 16.

$$Q(U) = m.(U - 1) \tag{16}$$

When using a deadband in the PID control method, the reactive power $Q(U)$ is determined by using Equation 17.

$$Q(U) = \begin{cases} Q_{MAX} \dfrac{U_{d,min} - U}{U_{d,min} - U_{min}} & if U < U_{d,min} \\ 0 & if\ U_{d,min} \leq U \leq U_{max} \\ Q_{min} \dfrac{U_{d,min} - U}{U_{d,max} - U_{max}} & if\ U > U_{d,max} \end{cases} \quad (17)$$

A deadband that is too wide can lead to undesirable outcomes. Specifically, inverters located closer to the transformer station may not participate effectively in voltage regulation, while those situated at the far ends of the network may be required to provide maximum reactive power.

2.3.2 Power Factor Based on Active Power

Photovoltaic (PV) systems are required to generate negative reactive power to counteract voltage increases caused by the injection of active power. Utilizing a PID control approach, inverters adjust the supplied reactive power based on measured voltage variations. Unlike the Q(U) algorithm, where the inverter located farthest from the transformer tends to supply more reactive power compared to those closer to the transformer, PID control offers a more balanced approach. This method ensures better overall voltage regulation as all inverters within the network actively participate in the voltage control process. However, a drawback of this method is that the inverters may supply reactive power even when it is not necessary, as there may be no overvoltage condition present.

The amount of reactive power to be supplied is determined according to a curve depicted in Figure 7. When the inverter's active power output is less than 0.5 pu, the power factor (PF) should be maintained at 1 pu. If the active power output exceeds 0.5 pu, the PID control will adjust to maintain a lagging power factor based on the curve's slope. The maximum power factor setting can be configured up to 0.90 or as required by the system. The detailed parameter settings used for each scenario, including voltage limits, reactive power limits, slope values, and deadband ranges, are shown in Table 3.

Table 3. Simulated Study Cases and Chosen Parameters for Q(U) Control Strategy

Ca -se	Penetrat-Ion(%)	U_{min} [pu]	U_{max} [pu]	Q_{min} [pu]	Q_{max} [pu]	M	U_{dmin} [pu]	U_{dmax} [pu]
1	0,10,50	1	1	0	0	0	1	1
2	0,10,50	0,8	1.2	-0.8	0.8	6	1	1
3	0,10,50	0,8	1.2	-0.8	0.8	7.6	0.97	1.02
4	0,10,50	0,8	1.2	-0.8	0.8	10	0.94	1.04
5	0,10,50	0,8	1.2	-0.47	0.47	4.8	1	1
6	0,10,50	0,8	1.2	-0.4	0.4	6	1	1

With 0.95 pu lagging, the PF(P) can be expressed by Equation 18.

$$tPF(P) = \begin{cases} 1 & P < 0.5 \\ \dfrac{P - 0.5}{10} = +0.95 & P \geq 0.5 \end{cases} \quad (18)$$

3. Results and Discussion

This case study is implemented using MATLAB simulations. The network consists of two LV feeders supplied by a single 100 kVA MV/LV transformer, with a power factor of 0.95. The PV inverters are modeled as controlled current sources, placed near each load.

In this research, PV peak capacity is defined as the installed PV capacity, while peak load refers to the maximum capacity of the PV inverter. For the LV network under study, it is expected that residential solar power systems will yield an installed capacity of 5 kVA. If all consumers on a residential feeder install a 5 kVA solar system, this would correspond to a 100% PV penetration on the respective feeder. This method of estimating PV hosting capacity in the network has the advantage of creating a uniform distribution of PV power across the entire feeder. Implementing PID control can optimize the system's performance by fine-tuning the necessary parameters to achieve better stability and efficiency.

Table 4. Simulated Study Cases and Chosen Parameters for PF (P) Control Strategy

Case	PV penetration	Min PF	Trafo(Kva)
7	0,8,60	0.94	100

Table 5. Different Scenarios

Scenario	PV[pu]	Load (kVA)
1	0.8	0.4
2	0	1.2

The simulated study cases presented in Table 3 for Q(U) and Table 4 for PF(P) illustrate various control approaches for PV inverters in an LV network. The transformer capacity used in the study is 100 kVA. In the base study case, Case 1, the PV inverters operate without any voltage control algorithm. Case 2 employs a Q(U) control algorithm, which exhibits high voltage sensitivity without a deadband. Cases 3 and 4 implement the Q(U) control algorithm with variations in the deadband, while Cases 5 and 6 show the Q(U) control algorithm without a deadband but with different voltage sensitivities compared to Case 2. Case 7 adopts the PF(P) control algorithm, with a minimum power factor of 0.92 (lagging), allowing for a better comparison with Cases 5 and 6, which have minimum power factors of 0.89 and 0.92, respectively.

Each study case includes two scenarios, as outlined in Table 5. Scenario 1 focuses on peak PV power output (0.8 pu) with the lowest load (0.4 kVA), while Scenario 2 deals with the lowest PV power output (0 pu) with peak load (1.2 kVA). This allows for the calculation of the maximum voltage for each bus in Scenario 1 and the minimum voltage in Scenario 2.

In this context, PID control can be applied to optimize the system's response to voltage variations occurring under different scenarios. By precisely tuning the PID control parameters, more stable and efficient voltage regulation can be achieved in the LV network, even as PV penetration levels vary from 0 to 60%. Effective PID control implementation also aids in analyzing and comparing the impact of various voltage regulation techniques on PV penetration in the network, leading to more optimal and reliable power distribution.

3.1 Comparison of PID Control Performance in Systems Without Voltage Regulation and with Q(U) Control

It is assumed that the voltage on the low-voltage side of the 60/10 kV transformer is 0.994 pu under minimum load conditions and 0.9727 pu during peak load conditions, as illustrated in Figures 8 and 9. The 10/0.4 kV transformer has the capability to adjust its tap position, resulting in a voltage increase of up to +2.5% on the secondary side to compensate for voltage drops during peak load periods. However, in this study, the transformer tap position remained constant. Figures 8 and 9 present the maximum and minimum voltage levels at each bus on feeder 1 for case 1, with PV penetration levels varying from 0 to 60% in increments of 10%, as shown in Table 3.

It is clear that the largest voltage variations occur at the farthest distance from the transformer (Bus 6 in Figure 8). The minimum voltage value for a particular bus remains unchanged across all levels of PV penetration because, during peak load hours (at night), the PV inverter does not contribute to the system. However, as PV penetration increases to 60%, significant voltage variations become more pronounced during periods of high solar generation.

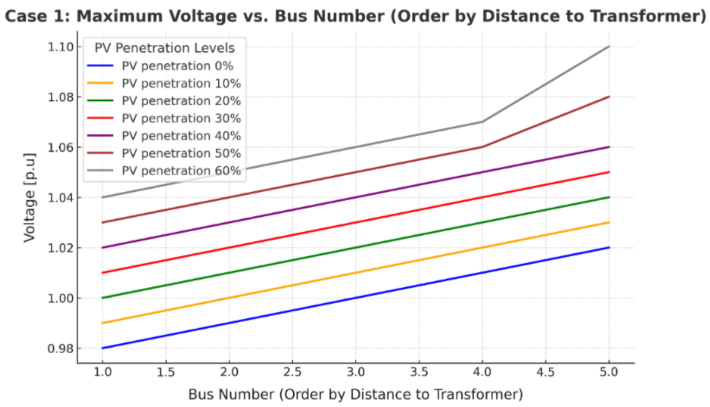

Figure 8. Study Case1-maximum Voltage for Each Bus for Variable PV Penetration

Figure 8 illustrates the relationship between maximum voltage (in pu) and bus number (ordered by distance from the transformer) at various levels of photovoltaic (PV) penetration, ranging from 0% to 60%. The horizontal axis represents the bus number, while the vertical axis represents the maximum voltage. Each colored line indicates a different level of PV penetration, showing a clear trend where the maximum voltage increases with higher PV penetration, especially for buses located far from the transformer. This shows that higher PV penetration has a significant impact on system voltage, especially at points far from the main power source.

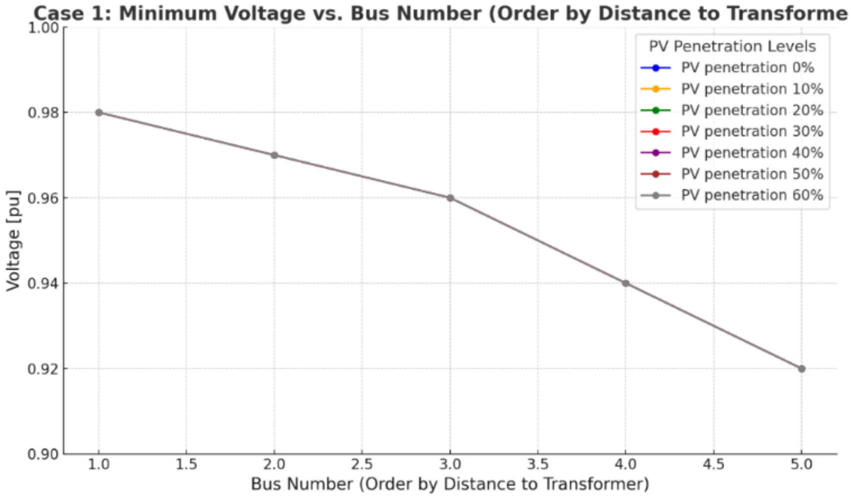

Figure 9. Study Case1-minimum Voltage for Each for Variable PV Penetration

Figure 9 shows the minimum voltage at each bus, ordered by distance from the transformer, for PV penetrations from 0% to 60%. The voltage decreases with distance, and higher PV penetration levels do not significantly improve the voltage profile. This indicates that, in Case 1, PV systems alone have limited impact on mitigating voltage drops along the feeder.

The scenario shows that with 60% PV penetration, the maximum voltage on Bus 5 increases significantly to reach approximately 1.095 per unit. This shows an increase of 11.7% compared to the basic condition of 0% PV penetration, where the voltage is 0.98 pu. For example, in Case 2, where the Q(U) control strategy is applied, Figure 10 illustrates the relationship between PV penetration level and voltage rise, especially on buses farther from the transformer.

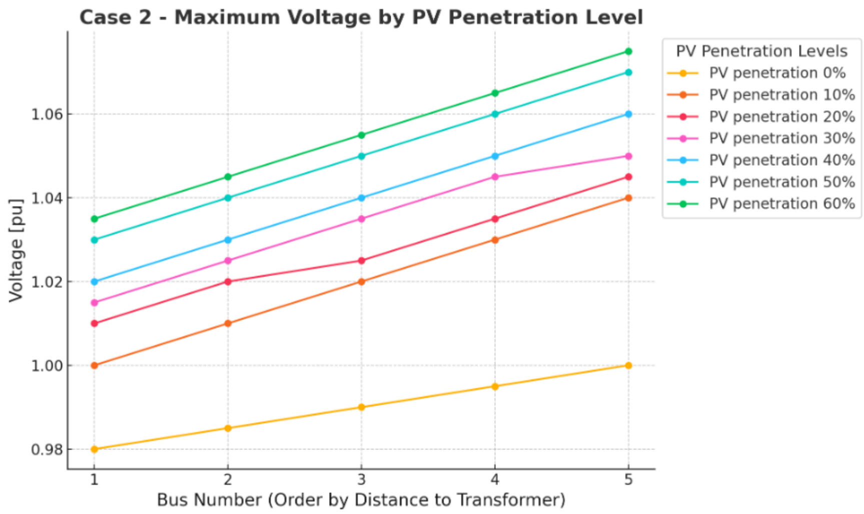

Figure 10. Study Case2-maximum Voltage for Each Bus for Variable PV Penetration

Voltage variations across buses follow similar trends without voltage regulation in Case 1. Increasing PV penetration to 60% leads to a maximum voltage rise of approximately 1.065 per unit at bus 5, representing an 8.7% increase compared to the scenario with 0% PV penetration. Additionally, as PV penetration increases, the minimum voltage for each bus also rises, thereby improving the overall voltage profile, as shown in Figure 11.

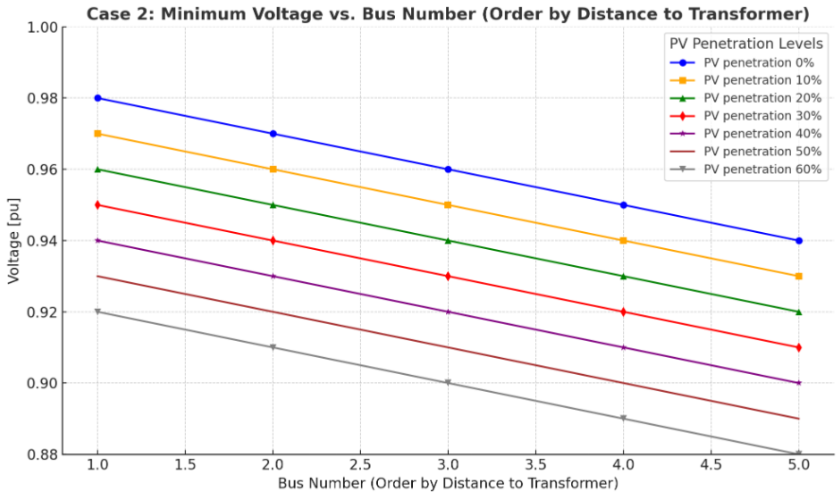

Figure 11. Study Case2-minimum Voltage for Each Bus for Variable PV Penetration

Figure 12 provides a comparison of the maximum and minimum voltage values for each bus with 60% PV penetration, clearly illustrating the voltage variation based on the bus number and the control method used. Two cases are compared, namely without control (Case 1) and with Q(U) control (Case 2). The results show that the Q(U) control method significantly improves the voltage profile at each bus compared to those without control, with higher and more stable voltages at all bus numbers. This improvement reflects the effectiveness of Q(U) control in maintaining voltage quality in the power system, especially at buses farther from the transformer, where voltage variations are more critical.

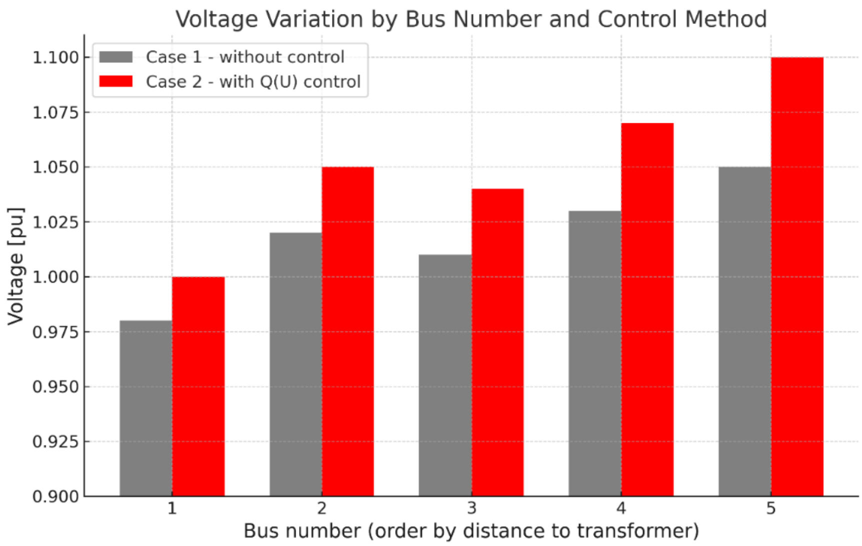

Figure 12. Comparison of Maximum/Minimum Voltage for Each Bus for 60% PV Penetration

Figure 13 shows the variation of maximum voltage at each bus based on PV (photovoltaic) penetration in Case 7. Each level of PV penetration (0% to 60%) results in an increase in voltage as the bus number increases, sorted by its distance from the transformer. This trend indicates that higher PV penetration tends to increase the overall voltage in the network, with a more significant impact on buses farther from the transformer.

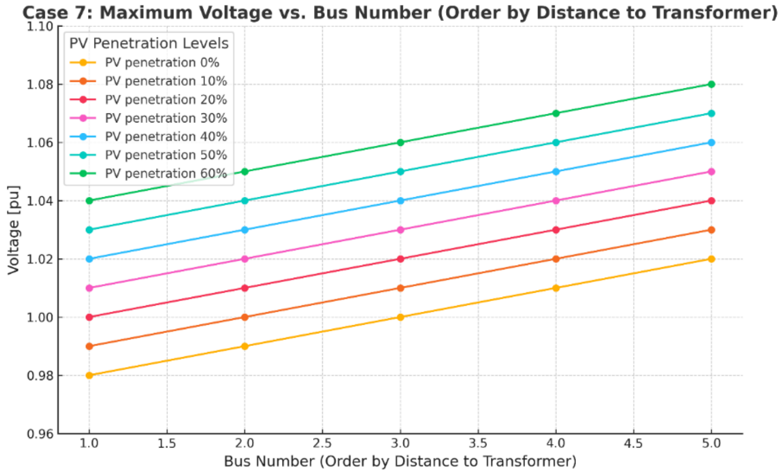

Figure 13. Study Mase7-maximum Voltage for Each Bus for Variable PV Penetration

Figure 14 shows the minimum voltage drop at each bus in the electrical system based on PV (Photovoltaic) penetration of 60%. The voltage drop becomes more significant as the bus number increases, which describes the distance of the bus from the transformer. This shows the effect of PV penetration on the system voltage quality.

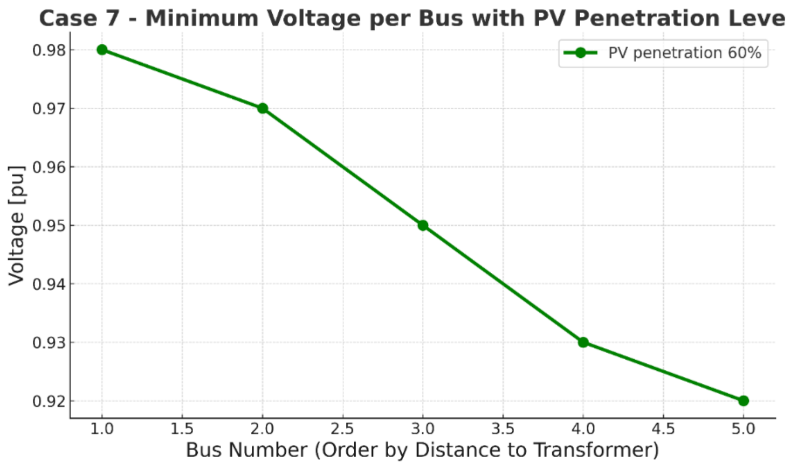

Figure 14. Study Case7-minimum Voltage for Each Bus for Variable PV Penetration

Figure 15 compares the voltage levels at each bus for two different control strategies, namely PF(P) in Case 7 and Q(U) in Case 2. The results show that the Q(U) strategy (blue) produces higher voltages at each bus compared to PF(P) (red). This difference becomes more significant at buses further from the transformer. This highlights the influence of control strategies on voltage stability in the power system.

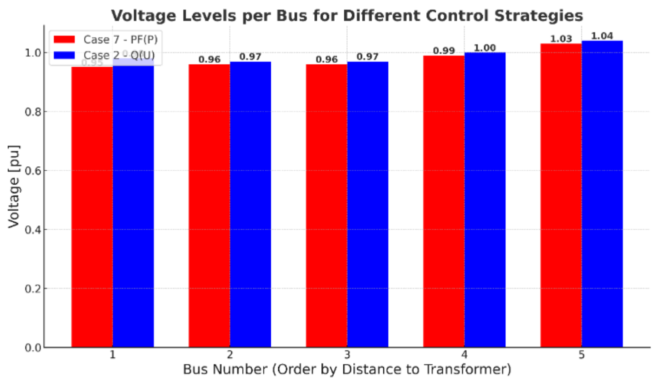

Figure 15. Comparison of Maximum/Minimum Voltage of Each Bus for 60% PV Penetration between Q(P) and PF (P)

Without the implementation of Q(U) control, the voltage at each bus exhibits significant fluctuations, particularly at bus 5 located at the end of the feeder, where voltage ranges from 0.92 pu to 1.09 pu. However, with the application of Q(U) control, the voltage variations across all buses are substantially reduced, thereby mitigating the impact of high PV penetration on the voltage profile, as illustrated in Figure 16.

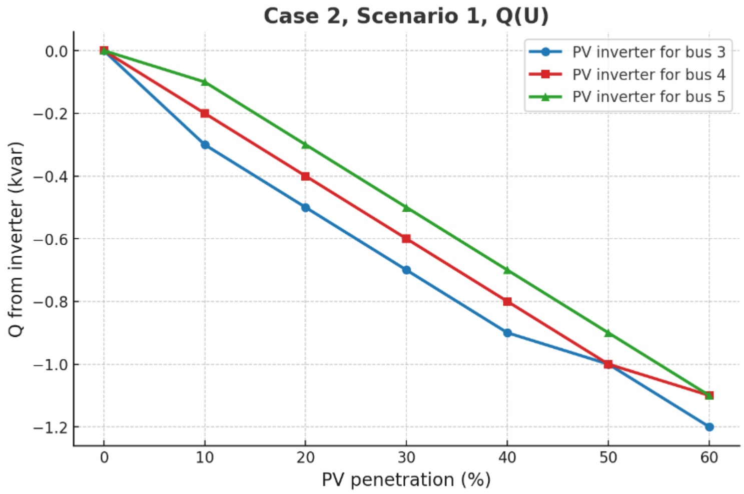

Figure 16. Study Case2-reactive Power for Inverters for Scenario1

3.2 Between Q(U) and PF(P) Control

In case 7, PF(P) control is adopted. Figures 13 and 14 display the maximum and minimum voltage for each bus under varying PV penetration levels with PF(P) control. It can be observed that the maximum voltage for each bus is very low because all inverters can inject the same maximum negative reactive power into the network according to the slope of the PF(P) curve. As PV penetration increases, the real power output of PV also increases, resulting in a lower power factor, and consequently, more reactive power is injected by the PV inverter.

Furthermore, it is also observed that the minimum voltage value for a specific bus remains the same across all PV penetration levels since, in scenario 2, the PV outputs no real power (at night), and thus the PV inverter does not inject reactive power.

A small comparison of the effectiveness between Q(U) and PF(P) control algorithms is shown in Figure 15. Cases 2 and 7 are selected because Case 2 corresponds to the most effective Q(U) voltage control method. It is evident that PF(P) control is more effective in lowering the maximum voltage at each bus due to its strong voltage control capability. However, Q(U) control contributes to raising the minimum voltage, whereas PF(P) has no influence on the minimum voltage.

3.3 Impact on Reactive Power and Line Losses

Figure 16 and Figure 17 illustrate the reactive power injected into the grid by inverters under different levels of PV penetration and various scenarios.

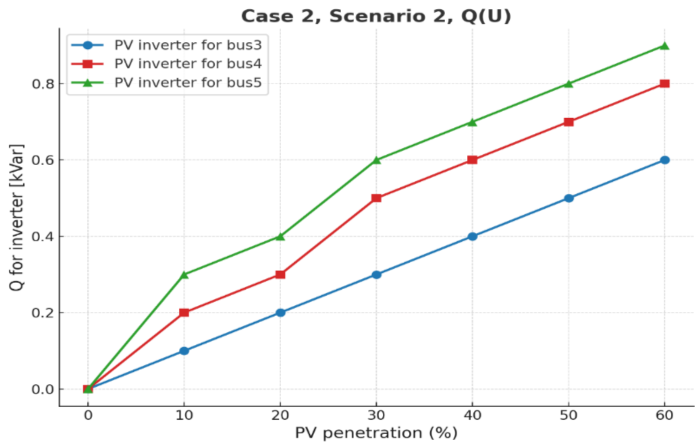

Figure 17. Study Case2-reactive Power for Inverters for Scenario2

From Q(U) Control, it can be observed that PV inverters inject negative inductive reactive power in scenario 1 because the voltage at each bus is higher than 1 pu, and inject positive inductive reactive power in scenario 2 due to the low voltage at each bus during peak load periods.

For scenario 1, the reactive power injected by the inverters varies according to the bus voltage, and the inverter for bus 5 injects the most reactive power compared to the other two inverters closer to the transformer. Reactive power injection is limited by the PV inverter's capacity and the Q(U) control slope. Since different PV penetration levels correspond to different PV inverter capacities, higher PV penetration leads to more reactive power being injected. In scenario 2, due to the low voltage profile in LV networks, all inverters will inject positive reactive power into the grid to improve the voltage profile. The PV inverter for bus 5 provides the maximum reactive power support due to the large voltage variation at bus 5, as shown in Figure 17.

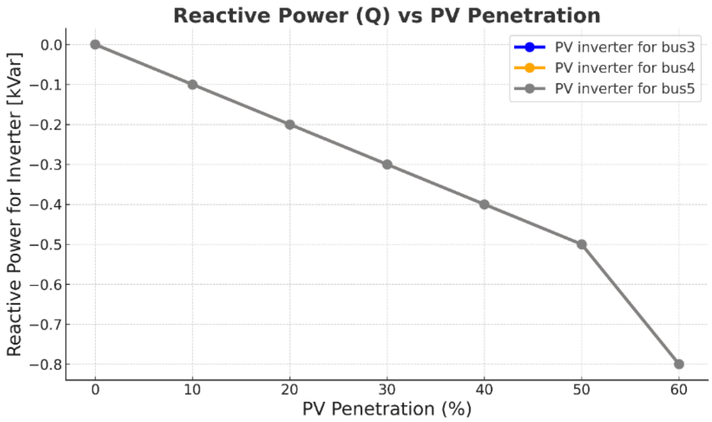

Figure 18. Study Case7-comparison of Reactive Power Injected by Inverter with Different Bus

With Q(U) control, inverters near the transformer are less effective in providing reactive power support to reduce the maximum voltage due to the small voltage fluctuation near the transformer, whereas PF(P) can provide the same reactive power support regardless of its location, as shown in Figure 18.

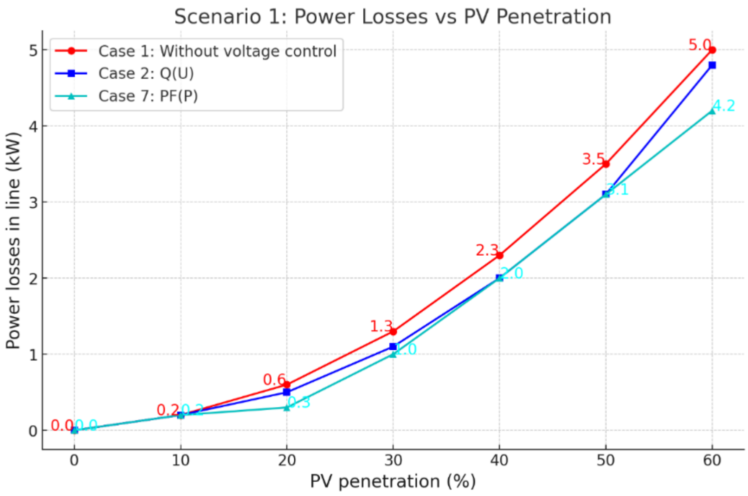

Figure 19. Total Line Losses for All Simulated Case

Figure 19 illustrates the power losses in lines for all simulated cases. The situation with no voltage control at all in the network would result in a total power loss of nearly 4.3 kW. For lower PV penetration levels, there are no significant differences among the simulated cases since the reactive power flow is also minimal. As the PV penetration level increases, different power losses can be observed due to the varying reactive power injection capabilities of different control methods. In all cases, a minimum power loss is achieved. At a 10% PV generation level, since the load demand is low in scenario 1, only a small amount of PV power is required to minimize power transfer in LV networks. When comparing Q(U) with PF(P), fewer power losses are achieved using Q(U) for PV penetration levels of 20%-50%.

However, for 60% PV penetration, the losses are almost the same. Compared to case 1 without voltage control, the losses increase by 28% for both Q(U) and PF(P) control.

3.4 Comparison of Hosting Capacity Across Different Cases

Table 6 presents the comparison of hosting capacities across the seven study cases. The cases are organized according to their hosting capacities, defined as the maximum PV penetration levels permissible within the allowed voltage variation limits. The first column highlights the hosting capacity from an overvoltage perspective, the second column lists the case numbers, and the third provides brief descriptions of each case. The fourth column indicates the maximum reactive power exchanged by the inverters, while the fifth column corresponds to the relevant power factor (PF).

Case 1 serves as the baseline scenario, with a hosting capacity of 36% (equivalent to 1.8 kW per household) without any reactive power control measures, resulting in minimal cable losses. Q(U) control with high sensitivity and a 4% dead-band, as seen in Case 3, achieves a hosting capacity of 40% (2 kW per household) and can be slightly increased by removing the dead-band, as demonstrated in Case 2. However, enlarging the dead-band, as done in Case 4, would reduce the hosting capacity. Although using Q(U) control with a dead-band may not reach a hosting capacity as high as without it, it results in lower line losses and can avoid unnecessary regulation, potentially offering additional advantages.

The hosting capacity further increases to 41.4% (2.07 kW per residence) while still maintaining a power factor above 0.92 in Case 6, by applying Q(U) control with low sensitivity. Q(U) control with medium sensitivity would achieve a higher hosting capacity than the one with low sensitivity because it can inject more reactive power into the grid, as demonstrated in Case 5. The penetration can be pushed further to 45% if the highest sensitivity is applied. However, line losses nearly double compared to the base case with only 36% penetration.

In case 7, using the standard PF(P) control increases the hosting capacity to 50% (2.5 kW per residence), but this also results in the highest line losses.

Thus, PF(P) control is generally assumed to provide better voltage management compared to Q(U), since all inverters in the network contribute to voltage control, regardless of the actual grid voltage. However, it also increases the hosting capacity. By applying PID control method to the inverter, a faster voltage response can be achieved compared to the methods proposed in the previous studies [29].

Table 6. Performance Comparison of Controller Response Times

Controller	Rise Time (s)	Seting Time	Overshoot (%)
PID	1.69	13.80	0.70
PI	1.64	38.11	68.78

Table 7 presents the response data of the PID controller compared to previous methods. Additionally, it highlights the comparison of voltage stability within the microgrid system. Meanwhile, Table 8 provides a comparison of power stability in the microgrid system.

Table 7. Power stability in Microgrid System

Parameter	PI	PID
Voltage(v)	194	220

The table highlights a comparison of output voltage in the microgrid system between PI and PID controllers. The PI controller recorded an output voltage of 194 V, which is lower than the PID controller's 220 V. This difference underscores the superior capability of the PID controller in maintaining voltage stability and achieving a value closer to the nominal level. This advantage is attributed to the PID controller's better dynamic response, including its ability to reduce overshoot, shorten settling time, and effectively handle disturbances compared to the PI controller. With more stable voltage closer to the nominal value, the PID controller is better suited for microgrid systems requiring high-precision control to ensure optimal performance of connected electrical devices.

4. Conclusion

Voltage regulation methods utilizing PV inverters, such as PF(P) and Q(U), are essential control systems that require precise parameter adjustments to ensure optimal voltage stability and performance in low-voltage networks. In this study, the analysis shows that the Q(U) control strategy consistently maintains higher voltage levels across all buses compared to PF(P), with improvements ranging from 0.03 pu at Bus 1 to 0.01 pu at Bus 5. These quantitative findings emphasize the effectiveness of Q(U) in achieving better voltage stability, particularly in networks with significant PV penetration.

By integrating a PID (Proportional-Integral-Derivative) control strategy into these methods, voltage regulation can be further optimized. The proportional component (P) of the PID controller minimizes voltage errors rapidly, while the integral component (I) corrects steady-state deviations caused by fluctuating loads or added PV capacity. Additionally, the derivative component (D) mitigates rapid voltage changes, preventing oscillations and enhancing stability.

Incorporating a well-tuned PID controller into PV inverter-based strategies such as Q(U) or PF(P) would improve the precision of parameter adjustments, allowing for adaptive and responsive voltage control. These enhancements would lead to more efficient and stable operations in low-voltage networks. By supporting higher renewable energy penetration, such methods can ensure reliable service quality while maintaining the system stability. This quantitative evidence highlights the need for advanced control mechanisms to meet the dynamic demands of modern power distribution systems.

References

[1] T. Jin, X. Shen, T. Su, and R. C. C. Flesch, "Model Predictive Voltage Control Based on Finite Control Set with Computation Time Delay Compensation for PV Systems," *IEEE Transactions on Energy Conversion*, vol. 34, no. 1, pp. 330–338, Mar. 2019. https://doi.org/10.1109/TEC.2018.2876619

[2] Z. Wang, Y. Yan, J. Yang, S. Li, and Q. Li, "Robust Voltage Regulation of a DC-AC Inverter with Load Variations via a HDOBC Approach," *IEEE Transactions on Circuits and Systems II: Express Briefs*, vol. 66, no. 7, pp. 1172–1176, Jul. 2019. https://doi.org/10.1109/TCSII.2018.2872330

[3] O. Ceylan, S. Paudyal, and I. Pisica, "Nodal Sensitivity-Based Smart Inverter Control for Voltage Regulation in Distribution Feeder," *IEEE J Photovolt*, vol. 11, no. 4, pp. 1105–1113, Jul. 2021. https://doi.org/10.1109/JPHOTOV.2021.3070416

[4] C. Yuan, X. Zhou, and Y. Ma, "DC Bus Voltage Control of Wind Power Inverter Based on First-Order LADRC," *IEEE Access*, vol. 10, pp. 3263–3274, 2022. https://doi.org/10.1109/ACCESS.2021.3138274

[5] G. Ding *et al.*, "Adaptive DC-Link Voltage Control of Two-Stage Photovoltaic Inverter during Low Voltage Ride-Through Operation," *IEEE Trans Power Electron*, vol. 31, no. 6, pp. 4182–4194, Jun. 2016. https://doi.org/10.1109/TPEL.2015.2469603

[6] N. Zhao, G. Wang, D. Xu, L. Zhu, G. Zhang, and J. Huo, "Inverter Power Control Based on DC-Link Voltage Regulation for IPMSM Drives Without Electrolytic Capacitors," *IEEE Trans Power Electron*, vol. 33, no. 1, pp. 558–571, Jan. 2018. https://doi.org/10.1109/TPEL.2017.2670623

[7] S. Y. M. Mousavi, A. Jalilian, M. Savaghebi, and J. M. Guerrero, "Autonomous Control of Current-and Voltage-Controlled DG Interface Inverters for Reactive Power Sharing and Harmonics Compensation in Islanded Microgrids," *IEEE Trans Power Electron*, vol. 33, no. 11, pp. 9375–9386, Nov. 2018. https://doi.org/10.1109/TPEL.2018.2792780

[8] M. Mehrasa, M. Sharifzadeh, M. Babaie, and K. Al-Haddad, "Power Sharing Management of a PEC9-based Microgrid by Feedback-Feedforward Control Strategy," 2020. https://doi.org/10.1109/ISIE45063.2020.9152380

[9] I. Sadeghkhani, M. E. H. Golshan, J. M. Guerrero, and A. Mehrizi-Sani, "A Current Limiting Strategy to Improve Fault Ride-Through of Inverter Interfaced Autonomous Microgrids," *IEEE Trans Smart Grid*, vol. 8, no. 5, pp. 2138–2148, Sep. 2017. https://doi.org/10.1109/TSG.2016.2517201

[10] J. Schiffer, T. Seel, J. Raisch, and T. Sezi, "Voltage Stability and Reactive Power Sharing in Inverter-Based Microgrids with Consensus-Based Distributed Voltage Control," *IEEE Transactions on Control Systems Technology*, vol. 24, no. 1, pp. 96–109, Jan. 2016. https://doi.org/10.1109/TCST.2015.2420622

[11] K. Tian, B. Wu, M. Narimani, D. Xu, Z. Cheng, and N. R. Zargari, "A capacitor voltage-balancing method for nested neutral point clamped (NNPC) Inverter," *IEEE Trans Power Electron*, vol. 31, no. 3, pp. 2575–2583, Mar. 2016. https://doi.org/10.1109/TPEL.2015.2438779

[12] L. Zhang, K. Sun, M. Gu, D. Xu, and Y. Gu, "A capacitor voltage balancing control method for five-level full-bridge grid-tied inverters without split-capacitor voltage sampling," *IEEE J Emerg Sel Top Power Electron*, vol. 6, no. 4, pp. 2042–2052, Dec. 2018. https://doi.org/10.1109/JESTPE.2017.2785819

[13] X. Zhou and S. Lu, "A novel inverter-side current control method of LCL-Filtered inverters based on high-pass- filtered capacitor voltage feedforward," *IEEE Access*, vol. 8, pp. 16528–16538, 2020. https://doi.org/10.1109/ACCESS.2020.2967122

[14] R. Guzman, L. G. De Vicuna, M. Castilla, J. Miret, and H. Martin, "Variable structure control in natural frame for three-phase grid-connected inverters with LCL filter," *IEEE Trans Power Electron*, vol. 33, no. 5, pp. 4512–4522, May 2018. https://doi.org/10.1109/TPEL.2017.2723638

[15] H. A. Young, V. A. Marin, C. Pesce, and J. Rodriguez, "Simple Finite-Control-Set Model Predictive Control of Grid-Forming Inverters with LCL Filters," *IEEE Access*, vol. 8, pp. 81246–81256, 2020. https://doi.org/10.1109/ACCESS.2020.2991396

[16] Z. Zhou, X. Li, Y. Lu, Y. Liu, G. Shen, and X. Wu, "Stability Blind-Area-Free Control Design for Microgrid-Interfaced Voltage Source Inverters under Dual-Mode Operation," *IEEE Trans Power Electron*, vol. 35, no. 11, pp. 12555–12569, Nov. 2020. https://doi.org/10.1109/TPEL.2020.2988565

[17] Y. Jia, J. Zhao, and X. Fu, "Direct grid current control of LCL-filtered grid-connected inverter mitigating grid voltage disturbance," *IEEE Trans Power Electron*, vol. 29, no. 3, pp. 1532–1541, 2014. https://doi.org/10.1109/TPEL.2013.2264098

[18] Y. Zhu and J. Fei, "Disturbance Observer Based Fuzzy Sliding Mode Control of PV Grid Connected Inverter," *IEEE Access*, vol. 6, pp. 21202–21211, Apr. 2018. https://doi.org/10.1109/ACCESS.2018.2825678

[19] R. J. Wai, Y. F. Lin, and Y. K. Liu, "Design of Adaptive Fuzzy-Neural-Network Control for a Single-Stage Boost Inverter," *IEEE Trans Power Electron*, vol. 30, no. 12, pp. 7282–7298, Dec. 2015. https://doi.org/10.1109/TPEL.2015.2396891

[20] S. Ghosh and S. Chattopadhyay, "Three-loop-based universal control architecture for decentralized operation of multiple inverters in an autonomous grid-interactive microgrid," *IEEE Trans Ind Appl*, vol. 56, no. 2, pp. 1966–1979, Mar. 2020. https://doi.org/10.1109/TIA.2020.2964746

[21] M. M. Hashempour, M. Y. Yang, and T. L. Lee, "An Adaptive Control of DPWM for Clamped-Three-Level Photovoltaic Inverters with Unbalanced Neutral-Point Voltage," in *IEEE Transactions on Industry Applications*, Institute of Electrical and Electronics Engineers Inc., Nov. 2018, pp. 6133–6148. https://doi.org/10.1109/TIA.2018.2849062

[22] R. O. Pratama, M. Effendy, and Z. Zulfatman, "Optimization of Maximum Power Point Tracking (MPPT) Using P&O-Fuzzy and IC-Fuzzy Algorithms on Photovoltaic," *Kinetik: Game Technology, Information System, Computer Network, Computing, Electronics, and Control*, pp. 119–134, Apr. 2018. https://doi.org/10.22219/kinetik.v3i2.200

[23] *Robust IDA-PBC based Load Voltage Controller for Power Quality Enhancement of Standalone Microgrids*. Institute of Electrical and Electronics Engineers, 2018.

[24] *MicrogridStability Enhancement by using Coordination of SFCL, SMES and Distributed Generation Units with Fuzzy Logic Controller : proceedings : Technology, Knowledge, and Society : 17-20 October 2019, Grand Hyatt Kochi Bolgatti, Kerala, India*. IEEE, 2019.
[25] A. Kusmantoro, "Coordinated Control of AC Microgrid for Increase Load Power Using Multi-Inverter," in *Proceedings - IEIT 2023: 2023 International Conference on Electrical and Information Technology*, Institute of Electrical and Electronics Engineers Inc., 2023, pp. 311–317. https://doi.org/10.1109/IEIT59852.2023.10335575
[26] A. Kusmantoro, "Multi-Inverter Coordinated Control on AC Microgrid for Increased Load Power," in *2023 6th International Conference on Vocational Education and Electrical Engineering: Integrating Scalable Digital Connectivity, Intelligence Systems, and Green Technology for Education and Sustainable Community Development, ICVEE 2023 - Proceeding*, Institute of Electrical and Electronics Engineers Inc., 2023, pp. 90–95. https://doi.org/10.1109/ICVEE59738.2023.10348326
[27] *Increasing PV Penetration Level in Smartgrid Systen Scenario by Enhancement of Reactive Power Suppor using Fuzzy Logic Controller*. Institute of Electrical and Electronics Engineers, 2018.
[28] A. Kusmantoro, "Real-Time Microgrid For Submersible Pump Energy Consumption Based On Fuzzy Logic Controller," in *2023 International Conference on Advanced Mechatronics, Intelligent Manufacture and Industrial Automation, ICAMIMIA 2023 - Proceedings*, Institute of Electrical and Electronics Engineers Inc., 2023, pp. 948–953. https://doi.org/10.1109/ICAMIMIA60881.2023.10427800
[29] A. Kusmantoro, A. Priyadi, V. L. Budiharto Putri, and M. Hery Purnomo, "Coordinated Control of Battery Energy Storage System Based on Fuzzy Logic for Microgrid with Modified AC Coupling Configuration," *International Journal of Intelligent Engineering and Systems*, vol. 14, no. 2, pp. 495–510, 2021. https://doi.org/10.22266/ijies2021.0430.45
[30] S. R. Das, P. K. Ray, A. Mohanty, and G. Panda, "Power Quality Enhancement in PV and Battery Storage Based Microgrid Using Hybrid Active Filter," in *3rd International Conference on Energy, Power and Environment: Towards Clean Energy Technologies, ICEPE 2020*, Institute of Electrical and Electronics Engineers Inc., Mar. 2021. https://doi.org/10.1109/ICEPE50861.2021.9404453
[31] A. Kusmantoro, "Enhancement DC Microgrid Power Stability with a Centralized," in *2022 5th International Conference on Vocational Education and Electrical Engineering: The Future of Electrical Engineering, Informatics, and Educational Technology Through the Freedom of Study in the Post-Pandemic Era, ICVEE 2022 - Proceeding*, Institute of Electrical and Electronics Engineers Inc., 2022, pp. 141–145. https://doi.org/10.1109/ICVEE57061.2022.9930460
[32] S. Mahdavi, H. Panamtash, A. Dimitrovski, and Q. Zhou, "Predictive Coordinated and Cooperative Voltage Control for Systems with High Penetration of PV," *IEEE Trans Ind Appl*, vol. 57, no. 3, pp. 2212–2222, May 2021. https://doi.org/10.1109/TIA.2021.3064910
[33] *Power Quality Enhancement of Micro-Grid Using DG and Power Quality Conditioner: 22-24, February 2017, SVS College of Engineering, Coimbatore, Tamil Nadu, India*. IEEE, 2017.
[34] *Voltage Stability in DC Micro Grid By Controlling Two Battery Units With Hybrid Network Systems 2019 International Conference on Technologies and Policies in Electric Power & Energy*. IEEE, 2019.
[35] *Fuzzy-PID Controller On MPPT PV To Stabilize DC Bus Voltage : 2018 International Conference on Control, Power, Communication and Computing Technologies (ICCPCCT)*. IEEE, 2018.
[36] *Distributed Power Quality Enhancement Using Residential Power Routers:2017 IEEE PES Innovative Smart Grid Technologies Conference Europe (ISGT-Europe) : conference proceedings : Torino, Italy, 26-29 September 2017*. IEEE, 2017.
[37] M. Mehrasa, M. Sharifzadeh, M. Babaie, and K. Al-Haddad, "Dynamic Droop Control in Microgrid for Stability Enhancement Considering RES Variation," 2020.
[38] A. Mirzaee, "Power quality Enhancement in Islanded Microgrid."
[39] A. Mortezaei, M. G. Simoes, M. Savaghebi, J. M. Guerrero, and A. Al-Durra, "Cooperative Control of Multi-Master-Slave Islanded Microgrid with Power Quality Enhancement Based on Conservative Power Theory," *IEEE Trans Smart Grid*, vol. 9, no. 4, pp. 2964–2975, Jul. 2018. https://doi.org/10.1109/TSG.2016.2623673
[40] *2018 International Conference on Control, Power, Communication and Computing Technologies (ICCPCCT):Power Quality Compensation In Microgrid Using MFGTI*. IEEE, 2018.